Research Article

The Optimization of Sheet Forming on Residual Stress and Surface Roughness with Two Point Incremental Forming Process (TPIF) of Aluminum Alloy Parts

Suriya Prasomthong* and Keattipong Onbat
Department of Industrial Technology, Faculty of Industrial Technology, Nakhon Phanom University, Nakhon Phanom, Thailand

* Corresponding author. E-mail: suriya.p@npu.ac.th DOI: 10.14416/j.asep.2022.06.003
Received: 23 February 2022; Revised: 30 March 2022; Accepted: 19 May 2022; Published online: 13 June 2022

Abstract
This study investigates the residual stress and surface roughness of AA5052 aluminum alloy with two points incremental forming (TPIF) processed. The experimental tool used for forming was a ball-shape tool for the truncated cone geometry of workpieces and forming by CNC machines. The residual stress was measured using the experimental forming tool. The residual stress was measured using the X-ray diffraction method. This study aimed to optimize the parameters using the Taguchi and analysis of variance (ANOVA) techniques. The TPIF process parameters include tool rotation speed and incremental depth. The results revealed that the optimal parameter obtained for the lowest residual stress and surface roughness were A1B1 (Rotation speed 0 rpm and Incremental depth 0.3 mm) with residual stress of 21.14 MPa and 0.46 μm of surface roughness. According to the results obtained by ANOVA, it was found that the rotation speed was significant to residual stress and incremental depth insignificant to residual stress. On the other hand, the most significant factor for surface roughness was incremental depth, but rotation speed was insignificant to surface roughness of formed parts at 95% confidence level.

Keywords: Two-point incremental forming (TPIF), Residual stress, X-ray diffraction

1 Introduction

Simple forming tools and equipment allow complex workpieces to be produced quickly using incremental sheet forming (ISF). The ISF process is applied for specific products, such as aerospace or specimens [1]. The forming equipment only includes the forming tool, plate clamping device (blank holder), and machines that can be used in computer numerical control (CNC) to produce workpieces with the desired shape [2], [3]. ISF is classified into two types: 1) a single point incremental forming (SPIF) process is a forming technique where the sheet metal is formed. It changes shape according to the direction of movement of the forming tool without a partial die and the blank holder movement during forming, as shown in Figure 1(a), 2) Two-point incremental forming (TPIF) process will have different characteristics from SPIF is usually equipped with a partial die, and the blank holder can move in the direction of forming press as shown in Figure 1(b) [4]. Both ISF processes produce workpieces by causing the material to be continuously elongated with an incremental depth at a certain distance. Permanent deformation caused by stress conditions on the metal surface leading to spring back or even fatigue damage [5]–[7]. This will follow in case of improper selection of machining variables as the resulting stress is often influenced by process parameters, such as the rotation speed, feed rate, incremental depth, or tool radius. All these factors cause accumulated or residual stresses and surface roughness on the workpiece after forming [8]–[10]. Residual stress is caused by the operation or the manufacturing process. When the workpiece has residual stress that is too high, it will affect the life of the part.

Residual stress is measured in ISF processes

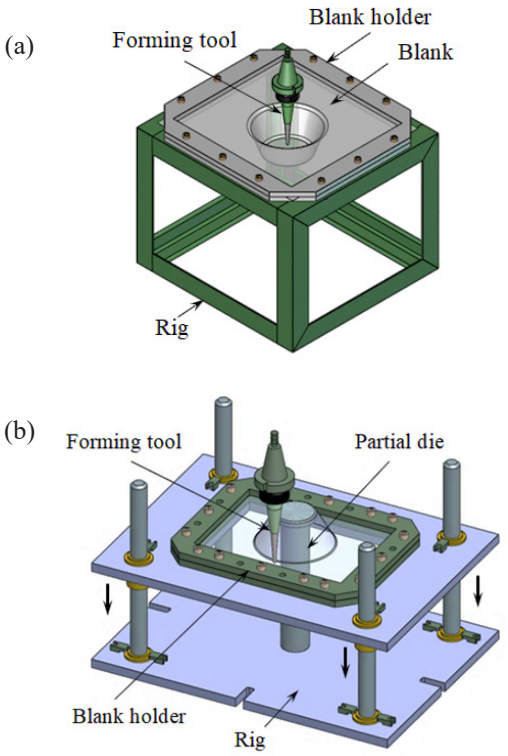

Figure 1: Schematic representation of the experimental setup for incremental sheet forming process variants, (a) Single point incremental forming (SPIF) and (b) Two-point incremental forming (TPIF) [4].

using X-ray diffraction techniques [11] by Slota *et al.* [12], where the residual stresses of conical specimens were analyzed by the SPIF process. The machining factors were studied and measurements were taken. The residual stress was obtained by the X-ray diffraction technique, where the mean stress was 84.5 MPa. Tanaka *et al.* [13] examined the residual stress of the SPIF extruded aluminium specimen using the X-ray technique. Diffraction by studying the tool radius and the feed rate affecting residual stress. Maaß *et al.* [14] investigated the influence of tool path strategies on residual stress by SPIF forming using the X-ray diffraction technique to check that the tool path does not affect the residual stress much. There are several studies that discuss the influence of SPIF forming factors on the residual stress of the workpiece after machining [15]–[17].

Currently, a wide range of studies has suggested experimental design guidelines for predicting and optimizing SPIF forming to achieve the desired objectives. Bahloul *et al.* [18] study SPIF forming parameters including wall angle, tool size, material thickness, and vertical step size by using statistical experimental design and the application of response surface metrology (RSM) to generate quadratic modeling of the Box-Behnken response. It was found that the model created was able to predict the response of the SPIF process effectively. Azhiri *et al.* [19] investigated parameters on the SPIF aluminum alloy forming process. The parameters in the study were the type of the tool, feed rate, and step down on the surface roughness. Design experiments were conducted with full factorial experimental design to optimize process parameters. It was found that the optimal parameters were the ball nose tool, 200 mm/min of feed rate and 0.4 mm of a step-down. Mulay *et al.* [20] constructed a predictive model using an artificial neural network (ANN) of the SPIF process for forming AA5052-H32 aluminum alloy on surface roughness. It was found that the developed ANN model was able to accurately predict the response of the process. Sbayti *et al.* [21] Experimental design of a Box–Behnken with Response surface methodology (RSM) for predicting the final geometry of specimens with the SPIF processed. The investigation revealed that the model created was able to accurately predict the response. Najm *et al.* [22] studied the influence of forming tool characteristics on the surface smoothness of aluminum by SPIF forming process. A response prediction model was created with ANN and SVR. It was found that the model was able to accurately predict surface roughness. There is also a wide range of research that discusses predicting the response of SPIF processes.

Preliminary research shows that most studies focus on residual stress in SPIF forming, but not much on TPIF formed components. Therefore, this research has applied the above principles and concepts to the study of the TPIF process in aluminum forming AA5052. Forming parameters including rotation speeds and incremental depth, experimental design and S/N Ratio analysis using Taguchi method [23], [24], and Analysis of variance (ANOVA) for predicting residual stress and surface roughness. It also generates computational regression equations to predict rotation speeds and incremental depth that affect residual stress and surface roughness of AA5052 aluminum alloy parts produced from TPIF. The Taguchi method will be

able to design a TPIF. molding process efficiently and will be useful for manufacturers and those interested in further study of the TPIF forming process.

2 Materials and Methods

2.1 *Materials and TPIF process*

The experimental material is aluminum alloy AA5052, size 300 × 300 mm, thickness 1 mm. The chemical composition and mechanical properties are shown in Tables 1 and 2. The fixing on the device as shown in Figure 1(b), forms a cone at an angle of 25 degrees, the outer diameter of the cone 100 mm, the inner diameter of the cup 50 mm, the height of the cone 60 mm. The workpiece wall with the highest stress deformation is cut to check the residual stress. The forming parameters and the test position are as shown in Figure 2. The forming tool is made of tool steel D2, where the tool radius is 10 mm, and 1 m/min of feed rate. The forming is done by a computer numerical control (CNC). Surface roughness is measured in the center of the workpiece. Use Mitutoyo surface roughness meter, model SJ-410, digital numeric display. It is measured in microns. At a resolution of 0.001 microns, the surface roughness can be displayed as Ra, Rmax, Rz.

Table 1: Chemical composition of AA5052 Aluminum alloy

Alloy	Element (%wt)							
	Si	Fe	Cu	Mn	Mg	Cr	Zn	Al
AA5052	0.25	0.40	0.10	0.10	2.21	0.17	0.10	Bal.

Table 2: Mechanical properties of AA5052 Aluminum alloy

Alloy	Mechanical Properties			
	Fu (MPa)	Fy (MPa)	E (GPa)	*v*
AA5052	335	141	70.3	0.33

2.2 *The X-ray diffraction technique*

The instrument was the X-Ray Diffract meter Model XRD 6100 2kw Shimadzu diffraction analysis machine, using the $\alpha - Cu$ with 40 kV and 30 mA electromagnetic radiation with a nickel target K – β. Diffraction plane test at a diffraction angle 2θ greater than 120 degrees. To determine the peak angle by scanning from 10–80 degrees. Residual stress analysis

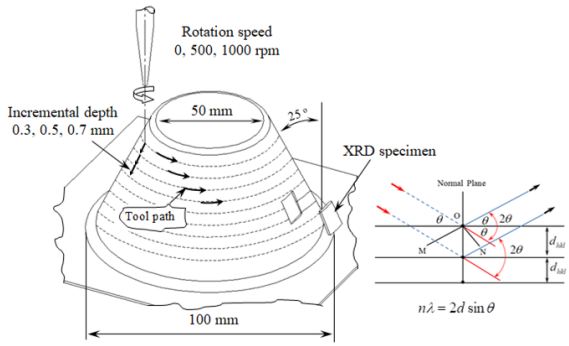

Figure 2: The experimental variables and the test position.

of TISF-formed specimens. Stress quantification was performed. Residue by measuring strain from peak broadening at half of the intensity peak makes use of the technique of Williamson-Hall: FWHM by determining the strain from the width peak along the angle 2θ. The microstrain can be calculated as in Equation (1), where β_T is total broadening, β_D is the broadening crystallite size and β_ε is the broadening to strain.

$$\beta_T = \beta_D + \beta_\varepsilon \tag{1}$$

Where the crystallite size β_D is calculated from the Scherrer formula as shown in Equation (2), where k is a dimensionless shape factor that has a value of about 0.9, λ the X-ray wavelength is 1.54056 nm, D is crystallite size, and 2θ is the diffraction angle.

$$D = \frac{k\lambda}{\beta_D \cos\theta} \text{ or } \beta_D = \frac{k\lambda}{D\cos\theta} \tag{2}$$

The microstrain case can be calculated from the equation $\beta_\varepsilon = 4\varepsilon \tan\theta$, so

$$\beta_T = \frac{k\lambda}{D\cos\theta} + 4\varepsilon\tan\theta \tag{3}$$

Where $\tan\theta = \sin\theta/\cos\theta$, then substitute the values in Equation (3) to get the Equation (4), yields

$$\beta_T = \frac{k\lambda}{D\cos\theta} + 4\varepsilon\frac{\sin\theta}{\cos\theta} \tag{4}$$

To solve the equation, Equation (5) was multiplied for both sides by $\cos\theta$, which is obtained in the form of the slope equation $y = mx + c$ where, $\beta_T \cos\theta = y$, $\varepsilon = m$, $4 \sin\theta = x$ and $k\lambda/D = c$

$$\beta_T \cos\theta = \varepsilon(4\sin\theta) + \frac{k\lambda}{D} \quad (5)$$

The mean residual stress was calculated and obtained by adjusting the linear equation with the least squares from the graph $\beta_T \cos\theta$ and 4 sin θ, and then use Equation (6) for residual stress calculation, where σ_ϕ is the stress after ascent. The figure, E is the elastic modulus, v is Poisson's ratio and m is the slope of the linear equation between $\beta_T \cos\theta$ and 4 sin θ

$$\sigma_\phi = \left(\frac{E}{\nu+1}\right)m \quad (6)$$

2.3 *Factor analysis in the forming process*

The TPIF process factor analysis uses the Taguchi method for designing and experimenting until finding out results obtained from the input factors. The tool used for the Taguchi method is the orthogonal array, a matrix system of the number of requirements at the row and column level. Taguchi method was applied to use the signal-to-noise ratio (S/N ratio) to find the number of available variables. The signal-to-noise ratio is the average measure of the effect of noise factors. It measures the S/N ratio of the number of variables in the feedback data and brings it closest to the mean of the desired target response. The S/N ratio is a combination of the mean and standard deviation of the measurements of the analyzed data. The S/N ratio for this study was selected as an experimental target, the smaller ratio is better following the Equation (7). Ultimately, the result is the residual stress and surface roughness on the workpiece after forming. The used orthogonal array L-9 (3^2) was 9. The experiment of the orthogonal array sequencing was used to study the factors, as shown in Table 3.

$$S/N_s = -10\log\left(\frac{1}{n}\sum_{i=1}^{n} y_i^2\right) \quad (7)$$

Where S/N_s are signal-to-noise ratio, n is the number of data and y_i is the responses.

Table 3: Designs of factors and parameters used in the experiment

Experimental Factors	Experimental Level		
	–1	0	1
Rotation speed: (rpm)	0	500	1000
Incremental depth: (mm)	0.30	0.50	0.70

3 Results and Discussion

3.1 *X-Ray Diffraction technical*

The micro residual stress of AA5052 aluminum alloy was studied in a TPIF experiment using X-Ray diffraction analysis principles. The peak values were measured in specimens. By calculating according to Equation (5), the calculation results are applied to create a linear equation to find the slope for stress assessment. Figure 3 shows XRD patterns of unprocessed AA5052 aluminum alloy parts. Peak was then measured to determine the FWHM according to the analytical theory of the Williamson and Hall method. The calculation results are shown in Table 4. Then, a graph was created to find the slope, as shown in Figure 4(a) and (b), and the them-value was taken. The residual stress was calculated according to Equation (6). It was found that the residual stress of the unformed AA5052 aluminum alloy was shown to be 15.86 MPa, and the residual stress measurement of the workpiece after forming was performed and evaluated in the same manner as for unprocessed parts.

Table 4: The results of micro stress analysis of informing aluminum

(hkl)	2θ	θ	FWHM (β_T) in degree	FWHM (radians) ($\times 10^{-3}$)	$\beta_T \cos\theta$ ($\times 10^{-3}$)	4 sin θ
111	38.29	0.33	0.18	3.22	3.05	1.31
200	44.53	0.39	0.19	3.34	3.09	1.52
220	64.84	0.57	0.22	3.94	3.32	2.14
311	77.89	0.68	0.13	2.26	1.75	2.51

XRD patterns of AA5052 after forming at a rotation speed of 0–1000 rpm and incremental depth of 0.3–0.7 mm. The XRD patterns showed a high crystalline (200) plane concentration, but upon forming, the crystalline planeness of aluminum was changed from the plane (200) to a high degree of crystallinity, which is a crystalline plane (220). Figure 3(b)–(d) is similar, after forming, the crystalline plane of aluminum changes from plane (200) to crystalline plane (220), but the peak intensity is different. Then, peak height was measured to determine the FWHM. The strain of the workpiece was estimated before creating a graph to determine the slope for residual stress calculation.

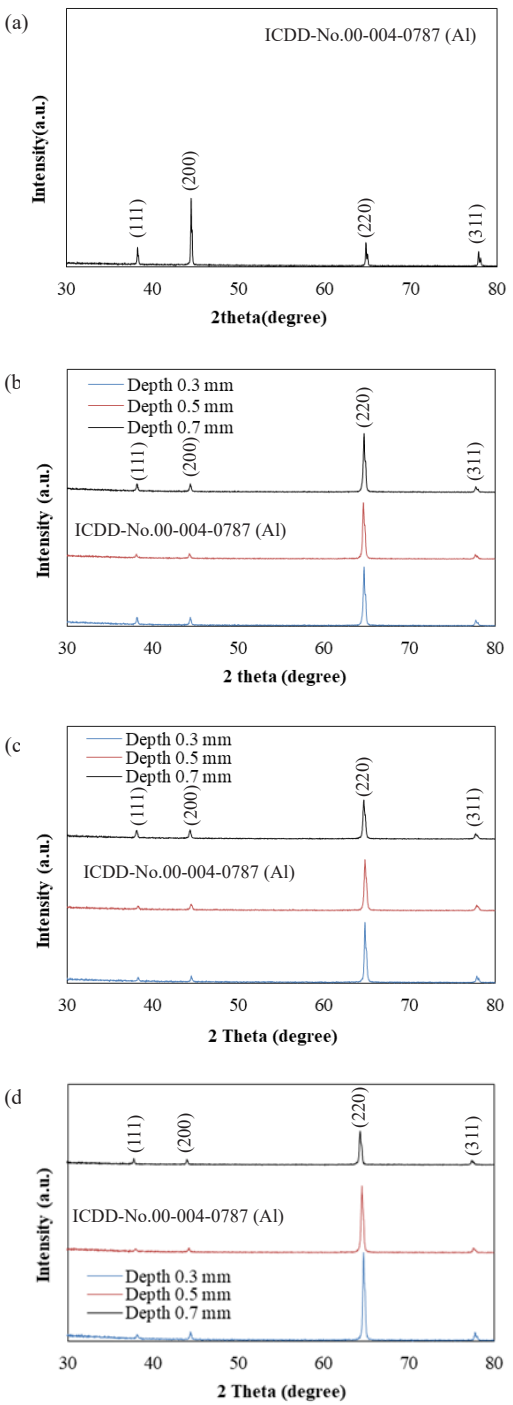

Figure 3: The XRD analysis (a) XRD patterns of AA5052 before forming (b) 0 rpm (c) 500 rpm and (d) 1000 rpm of rotation speed.

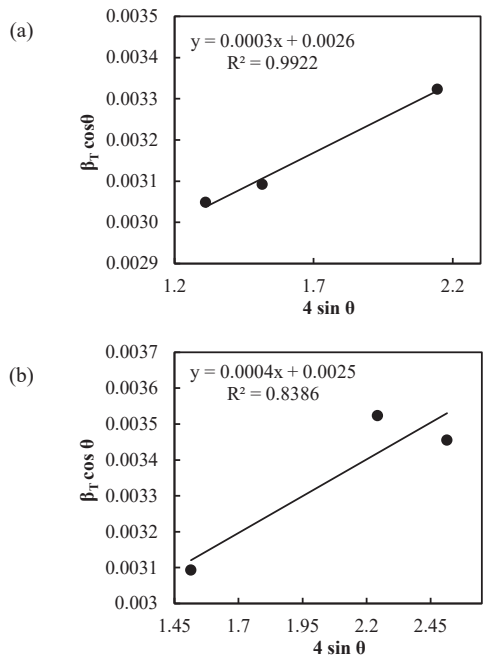

Figure 4: Plot of $\beta_T \cos\theta$ versus 4 sin θ (a) AA5052 before forming (b) 0 rpm and 0.3 mm of incremental depth.

3.2 *Signal-to-Noise Ratio (S/N Ratio)*

Signal-to-Noise Ratio (S/N Ratio) was analyzed at the process factor level; with the lowest S/N ratio indicating part quality after forming (less ratio is better). Therefore, the optimal factor of the TPIF process requires a variable with the lowest S/N value, as excessive residual stress and surface roughness do not benefit the part after forming. The equation used to calculate the S/N ratio is shown in Equation (7).

3.2.1 S/N Ratio for residual stress

In this study, TPIF process parameters on residual stress in post-forming parts were studied. The experimental model, the experimental results and the residual stress S/N ratio are shown in Table 5. The average S/N response of residual stress is shown in Table 6. From the study, it was found that the experiment that gave the least residual stress was Experiment 1 (A_1B_1), which was the rotation speed at 0 rpm and the incremental depth of 0.3 mm, the lowest residual stress was 21.14 MPa. The highest residual stress was found in Experiment 9

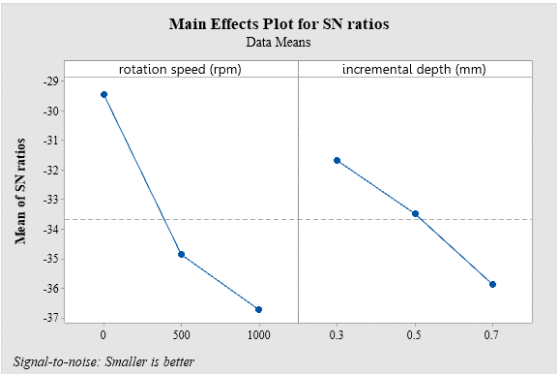

Figure 5: Main effects plot for the S/N ratio for residual stress.

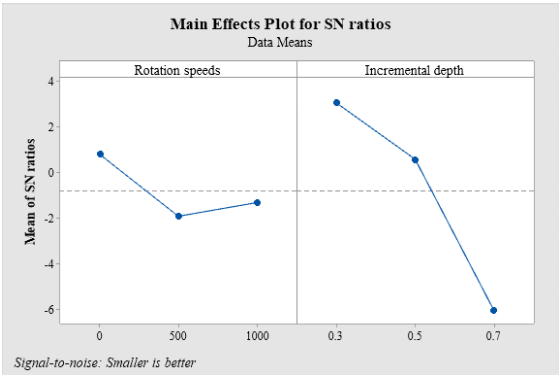

Figure 6: Main effects plot for the S/N ratio for Surface roughness.

(A_3B_3), with residual stress of 74.00 MPa at a forming rotation speed of 1000 rpm and an incremental depth of 0.7 mm. The other experimental sequences for each factor were shown in Table 5.

The main effect of the factor on the residual stress S/N ratio was predicted (Figure 5). The analysis results showed that the lowest S/N ratio of rotation speed was at level 1, 0 rpm, and the lowest S/N ratio of incremental depth was 0 at level 1, 0.3 mm. On the other hand, the maximum rotation speed S/N ratio is at level 3, 1000 rpm, and the maximum incremental depth S/N ratio at level 3 is 0.7 mm.

Table 5: Experimental layout: L9 orthogonal array, mean residual stress values, and S/N ratio values

Run	Rotation Speed (rpm) : A	Incremental Depth (mm) : B	Residual Stress (MPa)	SN-Ratio
1	**0**	**0.3**	**21.14**	**–26.5021**
2	0	0.5	26.40	–28.4321
3	0	0.7	47.00	–33.442
4	500	0.3	42.20	–32.5062
5	500	0.5	58.10	–35.2835
6	500	0.7	69.20	–37.9745
7	1000	0.3	63.40	–36.0418
8	1000	0.5	68.70	–36.7391
9	**1000**	**0.7**	**74.00**	**–37.3846**

Table 6 shows the response values of the S/N ratio to the residual stress of the factors at each level. The results of the analysis revealed that the rotation speed S/N ratio response was the lowest at Level 1, –29.46, and the Level 1 incremental depth S/N ratio response was the lowest at –31.68.

Table 6: Response table for S/N ratios of residual stress

Level	Rotation Speeds (rpm)	Incremental Depth (mm)
1	–29.46	–31.68
2	–34.86	–33.48
3	–36.72	–35.88
Delta	7.26	4.19
Rank	1	2

3.2.2 S/N Ratio for surface roughness (Ra)

The order of the experiments, the results and the S/N ratio of surface roughness are shown in Table 7. It was found that the experiments with the lowest surface roughness of the first experiment (A_1B_1) was a machining rotation speed of 0 rpm and an incremental depth of 0.3 mm. The minimum surface roughness was 0.46 µm, and the maximum surface roughness of the experiment was at sixth experiment (A_2B_3), a residual stress of 2.45 µm at a machining rotation speed of 500 rpm and incremental depth of 0.7 mm (Figure 6).

Table 7: Experimental layout: L9 orthogonal array, mean surface roughness values, and S/N ratio values

Run	Rotation Speed (rpm) : A	Incremental Depth (mm) : B	Surface Roughness (µm)	SN-Ratio
1	**0**	**0.3**	**0.46**	**6.69**
2	0	0.5	1.16	–1.32
3	0	0.7	1.40	–2.92
4	500	0.3	0.98	0.18
5	500	0.5	0.81	1.87
6	500	0.7	2.45	–7.78
7	1000	0.3	0.76	2.37
8	1000	0.5	0.87	1.22
9	**1000**	**0.7**	**2.37**	**–7.51**

Table 8 shows the response values of the S/N ratio to the Surface roughness of the factors at each level. The results of the analysis revealed that the rotation speed S/N ratio response was the lowest at Level 2, –1.9082, and the Level 3 incremental depth S/N ratio response was the lowest at –6.0701.

Table 8: Response table for S/N ratios of surface roughness

Level	Rotation Speeds (rpm)	Incremental Depth (mm)
1	0.8178	3.0804
2	–1.9082	0.5932
3	–1.3061	–6.0701
Delta	2.7260	9.1505
Rank	2	1

3.3 *Analysis of variance (ANOVA)*

Finding statistically significant factors using ANOVA on process parameter on response and the level of significance of factors considering ANOVA tables for a signal-to-noise ratio of mean residual stress and surface roughness of formed parts. The calculated values are given in Tables 9 and 10. An analysis of variance (ANOVA) found that rotation speed is significant on residual stress, and incremental depth is insignificant on residual stress. On the other hand, incremental depth is significant on surface roughness, and rotation speed is insignificant on average surface roughness at 95% confidence level.

Table 9: Analysis of variance for the S/N ratios for residual stress

Source	DF	Seq SS	Adj SS	Adj MS	F	P
Rotation speed	2	85.42	85.42	42.71	17.96	0.010
Incremental depth	2	26.54	26.54	13.27	5.58	0.070
Residual Error	4	9.51	9.51	2.38		
Total	8	121.47				

R-Sq = 92.17%; R-Sq (adj) = 84.34%

The analysis of variance for the S/N ratio, mean residual stress, was found that R-Sq = 92.17%, indicating that the factors were related. The parameter on residual stress is rotation speed with p-value < 0.05, indicating that the factor on residual stress is significant. An incremental depth p-value > 0.05 indicates that this factor insignificantly was residual stress at 95% confidence level, as shown in Table 9.

Table 10: Analysis of variance for the S/N for surface roughness

Source	DF	Seq SS	Adj SS	Adj MS	F	P
Rotation speed	2	12.30	12.30	6.152	0.81	0.505
Incremental depth	2	134.32	134.32	67.16	8.89	0.034
Residual Error	4	30.23	30.23	7.56		
Total	8	176.85				

R-Sq = 82.91%; R-Sq (adj) = 65.82%

Table 10 shows the results of ANOVA for the S/N ratio, mean surface roughness, R-Sq = 82.91%, indicating that the factors were related. The parameter affects on surface roughness is incremental depth, a p-value < 0.05 indicates that this factor significantly on surface roughness. Rotation speeds with a p-value > 0.05 indicate that this parameter insignificantly on surface roughness at a 95% confidence level.

3.4 *Regression analysis*

In order to establish a mathematical relationship between the parameters and residual stress, a regression analysis was carried out using the three uncoded parameters and their interactions. From the results of the experiments, the optimal FSW process parameters were coupled with the optimal residual stress when the rotational speed was at 0 rpm, and the incremental depth was at 0.3 mm. The predictive residual stress according to the Taguchi analysis was 21.55 MPa. Accordingly, a quadratic model, including linear and interaction terms, was developed, as shown in Equation (8).

$$\text{Residual stress} = 7.20 + 0.03719(\text{Rotation speed}) + 52.9\ (\text{Incremental depth}) \quad (8)$$

The predictive residual stress was

$$\text{Residual stress} = 7.20 + 0.03719(0) + 52.9\ (0.3) = 23.07 \text{ MPa}$$

From the results of the experiments, the optimal TPIS process parameters were coupled with the optimal surface rough when the rotational speed was at 0 rpm, and the incremental depth was at 0.3 mm. The surface roughness in the workpiece according to the Taguchi

analysis was 0.491 µm. accordingly, a quadratic model, including linear and interaction terms, was developed, as shown as Equation (9).

$$\text{Ra (µm)} = -0.586 + 0.000326\,(\text{Rotation speed}) + 3.350\,(\text{Incremental depth}) \quad (9)$$

The predictive surface rough was

$$\text{Ra (µm)} = -0.586 + 0.000326\,(0) + 3.350\,(0.3) = 0.419\ \text{µm}$$

Table 11 shows the results of the comparison of the experiments with the results of statistical analyzes. It was found that the confirmation of the experimental residual stress was a mean of 21.14 MPa. The predicted residual stress by the Taguchi method and the regression analysis was equal to 21.55 MPa and 23.07 MPa, respectively, for confirmation of surface roughness results were averaged at 0.46 µm. Taguchi residual stress predictions and regression analyses were 0.491 µm and 0.419 µm, respectively. Compared the results of the experiment with the results of statistical analysis of the results, it was found that the values were similar.

Table 11: Comparison of the experimental results with the statistical analysis of the response

Response	Statistical Analysis		Experimental
	Taguchi Model	Regression Analysis	
Residual stress (MPa)	21.55	23.07	21.14
Surface roughness (µm)	0.491	0.419	0.460

Table 12 summarizes the performances of the previous and proposed techniques. It was found that the research mentioned has a method for designing experiments with complexity and large sample size. As a result, the experiment is consumable and difficult to analyze data. The Taguchi method has the advantage of being able to reduce the sample size of the experiment. Where the Taguchi method was able to predict the results of the experiment effectively. Moreover, this research also studied the residual stress and surface roughness of the workpiece after forming for information in further research and study.

Table 12: Comparison method of residual stress and surface roughness based on aluminum alloy parts

Method	Material	Surface Roughness (µm)	Residual Stress (MPa)	Ref.
FEA techniques	Al/Cu bimetal	N/A	31	[17]
RSM/BBD	Al3003-O	N/A	N/A	[18]
ANFIS	AA5052	0.164	N/A	[19]
ANFIS	AA5052-H32	1.9	N/A	[20]
RSM/BBD	CP-Ti Gr	N/A	N/A	[21]
ANN	AlMn1Mg1	0.917	N/A	[22]
Taguchi	AA5052	0.460	21.14	This work

4 Conclusions

The TPIF process parameters using mean residual stress and surface roughness of S/N ratio values obtained the optimal level A_1B_1, which gave the predicted residual stress from the Taguchi model of 21.55 MPa, regression analysis was 23.07 MPa, and the experimental confirmation of residual stress was 21.14 MPa. Surface roughness was Taguchi model 0.491 µm, regression analysis 0.419 µm, and experimental confirmation was 0.460 µm at the same experimental factor level. An analysis of variance (ANOVA) found that the forming factor that was significant to residual stress was rotation speed and incremental depth insignificant to residual stress. On the other hand, the most significant factor for surface roughness was incremental depth, but rotation speed was insignificant to surface roughness of formed parts at a 95% confidence level. Future plans for the study should investigate the tensile strength and fracture mechanisms of the specimens to confirm the results against residual stresses.

Acknowledgments

The authors would like to gratitude the Faculty of Industrial Technology, Nakon Phanom University, Thailand for the experimental laboratory facilities. And would also like to give his sincere appreciation to Dr.Somchat Sonasang for his template manuscript of the revised manuscript to meet the journal standards.

Author Contributions

S.P.: conceptualization, research design, investigation,

methodology, software, writing-original draft preparation; K.O.: experimental setup and data analysis. All authors have read and agreed to the published version of the manuscript.

Conflicts of Interest

The authors declare no conflict of interest.

References

[1] N. A. Ismail, M. I. S. Ismail, M. A. M. Radzman, M. K. A. M. Ariffin, and A. As'arry, "Parametric optimization of robot-based single point incremental forming using Taguchi method," *International Journal of Integrated Engineering*, vol. 11, pp. 217–224, 2019.

[2] P. B. Uttarwar, S. K Raini, and D. S. Malwad, "Optimization of process parameter on surface roughness (Ra) and wall thickness on SPIF using Taguchi method," *International Research Journal of Engineering and Technology*, vol. 2, pp. 781–784, 2015.

[3] S. D. Majali, G. Chandramohan, and M. S. Kumar, "Effect of incremental forming process parameters on aluminum alloy using experimental studies," *Advanced Materials Research*, vol. 1119, pp. 633–639, 2015.

[4] M. B. Silva and P. A. F. Martins, "Two-point incremental forming with partial die: Theory and experimentation," *Journal of Materials Engineering and Performance*, vol. 22, pp. 1018–1027, 2013.

[5] F. Maqbool and M. Bambach, "Experimental and numerical investigation of the influence of process parameters in incremental sheet metal forming on residual stresses," *Journal of Manufacturing and Materials Processing*, vol. 3, no. 2, 2019, Art. no. 31.

[6] N. Huber and J. Heerens, "On the effect of a general residual stress state on indentation and hardness testing," *Acta Materialia*, vol. 56, pp. 6205–6213, 2008.

[7] M. Bambach, B. T. Araghi, and G. Hirt, "Strategies to improve the geometric accuracy in asymmetric single point incremental forming," *Production Engineering*, vol. 3, pp. 145–156, 2009.

[8] A. Subrahmanyam, R. Lingam, K. Hayakawa, S. Tanaka, and N. V. Reddy, "Experimental and numerical investigation of residual stresses in incremental forming," *Materials Transactions*, vol. 61, no. 2, pp. 228–233, 2020.

[9] N. Baak, M. Garlich, A. Schmiedt, M. Bambach, and F. Walther, "Characterization of residual stresses in austenitic disc springs induced by martensite formation during incremental forming using micromagnetic methods," *Materials Testing*, vol. 59, pp. 309–314, 2017

[10] H. K. Nirala and A. Agrawal, "Reprint of: Residual stress inclusion in the incrementally formed geometry using Fractal Geometry based incremental tool path," *Journal of Materials Processing Technology*, vol. 287, 2021, Art. no. 116623.

[11] S. Walzer, M. Liewald, N. Simon, J. Gibmeier, H. Erdle, and T. Böhlke, "Improvement of sheet metal properties by inducing residual stresses into sheet metal components by embossing and reforming," *Applied Science and Engineering Progress*, vol. 15, no. 1, 2022, Art. no. 5414, doi: 10.14416/j.asep.2021.09.006.

[12] J. Slota, B. Krasowski, A. Kubit, T. Trzepiecinski, W. Bochnowski, K. Dudek, and M. Neslušan, "Residual stresses and surface roughness analysis of truncated cones of steel sheet made by single point incremental forming," *Metals*, vol. 10, no. 2, 2020, Art. no. 237.

[13] S. Tanaka, T. Nakamura, K. Hayakawa, H. Nakamura, and K. Motomura, "Residual stress in sheet metal parts made by incremental forming process," *AIP Conference Proceedings*, vol. 908, no. 1, pp. 775–780, 2007, Art. no. 775.

[14] F. Maaß, M. Hahn, M. Dobecki, E. Thannhäuser, A. E. Tekkaya, and W. Reimers, "Influence of tool path strategies on the residual stress development in single point incremental forming," *Procedia Manufacturing*, vol. 29, pp. 53–58, 2019.

[15] F. Maaß, M. Hahn, and A. E. Tekkaya, "Interaction of process parameters, forming mechanisms, and residual stresses in single point incremental forming," *Metals*, vol. 10, no. 5, 2020, Art. no. 656.

[16] F. Maaß, S. Gies, M. Dobecki, K. Brömmelhoff, A. E. Tekkaya, and W. Reimers, "Analysis of residual stress state in sheet metal parts processed by single point incremental forming," *AIP Conference Proceedings*, vol. 1960, no. 1, 2018, Art. no. 160017.

[17] M. Alinaghian, I. Alinaghian, and M. Honarpisheh, "Residual stress measurement of single point incremental formed Al/Cu bimetal using incremental hole-drilling method," *International Journal of Lightweight Materials and Manufacture*, vol. 2, pp. 131–139, 2019.

[18] R. Bahloul, H. Arfa, and H. BelHadjSalah, "A study on optimal design of process parameters in single point incremental forming of sheet metal by combining Box–Behnken design of experiments, response surface methods and genetic algorithms," *The International Journal of Advanced Manufacturing Technology*, vol. 74, pp. 163–185, 2014

[19] R. B. Azhiri, F. Rahimidehgolan, F. Javidpour, R. M. Tekiyeh, S. M. Moussavifard, and A. S. Bideskan, "Optimization of single point incremental forming process using ball nose tool," *Experimental Techniques*, vol. 44, pp. 75–84, 2020

[20] A. Mulay, B. S. Ben, S. Ismail, and A. Kocanda, "Prediction of average surface roughness and formability in single point incremental forming using artificial neural network," *Archives of Civil and Mechanical Engineering*, vol. 19, pp. 1135–1149, 2019

[21] M. Sbayti, R. Bahloul, H. BelHadjSalah, and F. Zemzemi, "Optimization techniques applied to single point incremental forming process for biomedical application," *The International Journal of Advanced Manufacturing Technology*, vol. 95, pp. 1789–1804, 2018

[22] S. M. Najm and I. Paniti, "Predict the effects of forming tool characteristics on surface roughness of aluminum foil components formed by SPIF using ANN and SVR," *International Journal of Precision Engineering and Manufacturing*, vol. 22, pp. 13–26, 2021

[23] Z. Liu, B. Li, Y. L. Daniel, and P. Meehan, "Taguchi optimization of process parameters for forming time in incremental sheet forming process," *Materials Science Forum*, vol. 773, pp. 137–143, 2014

[24] P. Chinnaiyan and A. K. Jeevanantham, "Multi-objective optimization of single point incremental sheet forming of AA5052 using Taguchi based grey relational analysis coupled with principal component analysis," *International Journal of Precision Engineering and Manufacturing*, vol. 15, pp. 2309–2316, 2014.